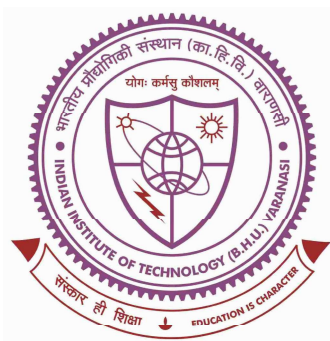


Traveling wave based protection and fault localization scheme for multi terminal HVDC grid and converter interfaced HVAC network



Thesis submitted in partial fulfillment
for the award of degree

Doctor of Philosophy

by

Mahitosh Banafer

DEPARTMENT OF ELECTRICAL ENGINEERING
Indian Institute of Technology
(Banaras Hindu University)
Varanasi

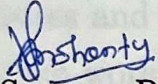
Roll No: 18081504

2023

Dedicated
To
My Parents &
Lord Vishwanath Ji

CERTIFICATE

It is certified that the work contained in the thesis titled **Traveling wave based protection and fault localization scheme for multi terminal HVDC grid and converter interfaced HVAC network** by **Mahitosh Banafer** has been carried out under my supervision and that this work has not been submitted elsewhere for a degree. It is further certified that the student has fulfilled all the requirements of Comprehensive Examination, Candidacy, and State of the Art (SOTA) for the award of Ph.D. Degree.



Dr. Soumya R. Mohanty

(Supervisor)

Department of Electrical Engineering
Indian Institute of Technology
(Banaras Hindu University)
Varanasi, India - 221005

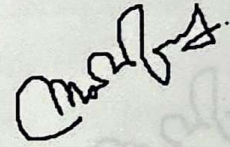
सहयुक्त आचार्य / ASSOCIATE PROFESSOR
विद्युतीय अभियान्तिकी विभाग/Department of Electrical Engineering
भारतीय प्रौद्योगिकी संस्थान/Indian Institute of Technology
(काशी हिन्दू विश्वविद्यालय)/(Banaras Hindu University)
Varanasi, U.P. (INDIA)

DECLARATION

I, Mahitosh Banafer, certify that the work embodied in this thesis is my own bonafide work and carried out by me under the supervision of Dr. Soumya R. Mohanty from 01-Jan-2019 to 20-October-2023, at the Department of Electrical Engineering, Indian Institute of Technology (BHU), Varanasi. The matter embodied in this thesis has not been submitted for the award of any other degree/diploma. I declare that I have faithfully acknowledged and given credits to the researchers wherever their works have been cited in this thesis. I further declare that I have not willfully copied any other's work, paragraphs, text, data, results, etc., reported in journals, books, magazines, reports, dissertations, thesis, etc., or available at websites and have not included them in this thesis and have not cited as my own work.

Date: 21-02-2024

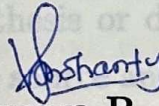
Place: Chennai



(Mahitosh Banafer)

CERTIFICATE BY THE SUPERVISOR

It is certified that the above statement made by the student is correct to the best of my/our knowledge.



Dr. Soumya R. Mohanty

Supervisor

सहयुक्त आचार्य / ASSOCIATE PROFESSOR
विद्युतीय अभियांत्रिकी विभाग / Department of Electrical Engineering
भारतीय प्रौद्योगिकी संस्थान / Indian Institute of Technology
(काशी हिन्दू विश्वविद्यालय) / (Banaras Hindu University)
Varanasi, U.P. (INDIA)

Signature of Head of Department/Coordinator of School

"SEAL OF THE DEPARTMENT/SCHOOL"

आचार्य व विभागाध्यक्ष / PROFESSOR & HEAD
विद्युतीय अभियांत्रिकी विभाग / Department of Electrical Engineering
भारतीय प्रौद्योगिकी संस्थान / Indian Institute of Technology
(काशी हिन्दू विश्वविद्यालय) / (Banaras Hindu University)
Varanasi, U.P. (INDIA)

COPYRIGHT TRANSFER CERTIFICATE

Title of the Thesis: **Traveling wave based protection and fault localization scheme for multi terminal HVDC grid and converter interfaced HVAC network**

Name of Student: **Mahitosh Banafer**

Copyright Transfer

The undersigned hereby assigns to the Indian Institute of Technology (Banaras Hindu University), Varanasi all rights under copyright that may exist in and for the above thesis submitted for the award of the Doctor of Philosophy.

Date: 21-02-2024

Place: Chennai



(Mahitosh Banafer)

Note: However, the author may reproduce or authorize others to reproduce material extracted verbatim from the thesis or derivative of the thesis for author's personal use provided that the source and the Institute's copyright notice are indicated.

Acknowledgments

First of all, I would want to begin by praising and thanking **Lord Vishwanath**, who has bestowed me with innumerable blessings, knowledge, and opportunities, allowing me to complete my thesis. Though, only my name appears on the cover of this dissertation, the success of this thesis rests heavily on the support and direction of many others. I owe my heartfelt gratitude to all those people who have made this thesis possible and because of whom my research experience has been one that I will cherish forever.

I would like to take this opportunity to thank and appreciate my supervisor, **Dr. Soumya R. Mohanty**, Electrical Engineering Department, IIT (BHU), Varanasi, for his exceptional guidance and constant encouragement throughout the course of this dissertation. I would like to express my deepest appreciation to **Dr. Soumya R. Mohanty** for his inspiration and helpful recommendations in completing my research work. I wish to extend my sincere gratitude towards my RPEC members, **Prof. M. K. Verma** as an internal expert and **Prof. Subir Das** as an external expert, for their help, valuable suggestions, and encouragement during the entire research work. I am grateful to my friend, **Dr. Tapan Prakash**, who provided me with technical, moral, and emotional support during my research program.

I would also like to thank, Head, Department of Electrical Engineering, Indian Institute of Technology (BHU), Varanasi, for providing all the facilities related to my research work. I wish to express my deep regards to, **Prof. S. P. Singh** for their unconditional support at every moment during the progress of my research. I also extend my heartfelt regards to all the faculty members of the Electrical Engineering Department.

I am also grateful to our laboratory staff, **Mr. Sanjay Singh and Mr. Dharmendra Singh**, for the assistance extended by them from time to time during this research work. I am grateful to all the office staff and authorities of the Department of Electrical Engineering, for their kind help during the period of my stay to complete the thesis work.

I am thankful to my fellow friends **Dr. Vivek Kumar, Mr. Ambuj Pandey, Mr. Rohit Kumar, Mr. Udit Prasad, Mrs. Babita Faujdar, Mr. Abhisek Singh and Mr. Alok Kumar** for the thought-provoking discussions, their support, cooperation and sincere help in many ways.

Last but not least, I will be eternally grateful to my entire family for their faith, patience, encouragement, blessings, and love. I am grateful to my father, **Mr. Manoj Kumar Banafer**; mother, **Mrs. Kusum Lata Banafer**; and sister **Ms. Kavita Singh Banafer**, for motivating, believing in, and strengthening me to fly high. A special thanks to my special family for always holding my hand through the ups and downs.

Date: 21-02-2024

Mahitosh Banafer

List of Tables

Table 2.1:	Parameters of MMC converter and AC/DC grid	21
Table 2.2:	Effect of Fault Location on Proposed Protection Scheme for DC Fault in Cable L_{34}	32
Table 2.3:	Effect of measurement noise and Fault impedance on Proposed Pro- tection Scheme for DC Fault at 50 km from DC Bus 3 in Cable L_{34}	36
Table 2.4:	Effect of Fault Location on Proposed Protection Scheme for DC Fault in Cable L_{34}	37
Table 2.5:	Comparative analysis with existing primary and backup protection scheme	40
Table 3.1:	MMC converter and AC/DC grid parameters	54
Table 3.2:	Impact of fault resistance on proposed TW based protection scheme	58
Table 3.3:	Impact of fault resistance on proposed TW based DC fault local- ization scheme	59
Table 3.4:	Impact of noise on proposed TW based protection scheme	61
Table 3.5:	Impact of measurement error on proposed TW based DC protection and fault localization scheme	62
Table 3.6:	Impact of Δt_{syn} on proposed TW based DC fault localization scheme	69
Table 3.7:	Impact of fault type on proposed TW based DC protection and fault localization scheme	71
Table 3.8:	Impact of external fault and DC grid parameter variation on pro- posed TW based DC protection scheme	73
Table 3.9:	Comparative analysis with existing protection and fault localization scheme	77

Table 4.1:	MMC converter and AC/DC grid parameters	93
Table 4.2:	Impact of fault location on proposed TW based fault localization scheme	95
Table 4.3:	Impact of fault resistance on proposed TW based fault localization scheme	96
Table 4.4:	Impact of noise on proposed TW based fault localization scheme	99
Table 4.5:	Impact of fault type on proposed TW based fault localization scheme	99
Table 5.1:	MMC converters and AC/DC grid parameters	118
Table 5.2:	Performance of proposed WABPS for different fault location in L_{23} (Fault distance is calculated from Bus 2)	121
Table 5.3:	Performance of wide area protection scheme for different fault location and fault impedance on transmission line and cable in L_{23} (Fault distance is calculated from Bus 2)	122
Table 5.4:	Performance of wide area protection scheme for different fault location and fault type in L_{23} (Fault distance is calculated from Bus 2)	124
Table 5.5:	Performance of proposed WABPS for different time synchronization error in L_{23} (Fault distance is calculated from Bus 2)	124
Table 5.6:	Performance of proposed WABPS for different FIA in L_{23} (Fault distance is calculated from Bus 2)	125
Table 5.7:	Performance of WABPS against LVRT control in MMC converter for fault in L_{12AC} and L_{23}	128

List of Figures

Figure 2.1:	MMC-MTDC test grid system.	20
Figure 2.2:	(a) Coupled wavelet decomposition scheme, (b) Two-level coupled wavelet decomposition scheme.	22
Figure 2.3:	(a) Measurement signal with 30 dB noise, (b) MMG output, (c) MUDW output.	24
Figure 2.4:	(a) DC substation protection unit layout, (b) Backup Protection logic diagram, (c) Proposed primary and backup protection scheme.	26
Figure 2.5:	Flowchart of the proposed primary and backup MTDC protection scheme.	29
Figure 2.6:	Performance of proposed MUDW based protection scheme (a) Mode-1 current at DC link L_{34} , (b) Polarity and AT of TW at CT_{34} , (c) Polarity and AT of TW at CT_{43} , (d) Mode-1 current at DC link L_{13} , (e) Polarity and AT of TW at CT_{13} , (f) , Polarity and AT of TW at CT_{31} , (g) Mode-1 current at DC link L_{42} , (h) Polarity and AT of TW at CT_{42} , (i) Polarity and AT of TW at CT_{24}	31
Figure 2.7:	(a) Noiseless Mode-1 current signal in CT24, (b) Mode-1 current signal in CT_{24} with 40 dB SNR, (c) Mode-1 current signal in CT_{24} with 30 dB SNR, (d) MUDW output for noiseless signal in CT_{24} , (e) MUDW output for signal with 40 dB SNR in CT_{24} , (f) MUDW output for signal with 30 dB SNR in CT_{24}	34

Figure 2.8: (a) Mode-1 current signal in CT_{24} with 10 Ω , 50 Ω and 100 Ω fault impedance, (b) MUDW signal output with 10 Ω fault impedance, (c) MUDW signal output with 50 Ω fault impedance, (d) MUDW signal output with 100 Ω fault impedance. 35

Figure 2.9: Effect of sampling frequency on AT of F_1 induced TW in (a) DC Link L_{34} , (b) DC Link L_{13} , (c) DC Link L_{42} 38

Figure 2.10: Comparison of Proposed MUDW protection scheme with MMG based protection scheme (a) Mode-1 current at both end of DC link L_{34} , (b) Polarity and AT of TW at CT_{34} , using MUDW (c) Polarity and AT of TW at CT_{43} using MUDW, (d) Mode-1 voltage at EPT_{34} , (e) Mode-0 voltage at EPT_{43} , (f) SATD difference between AT of TW between mode-1 and mode-0 signal using MMG technique. 39

Figure 3.1: (a) Fault induced TW in DC voltage, (b) TWAT determination using modified MMG output, (c) Proposed technique (based on modified MMG,sobel operator and linear regression) based AT detection for TW for low sampling frequency measurement, (d) Block diagram illustration of the performance of proposed AT detection technique under low sampling frequency measurement. 50

Figure 3.2: Two terminal DC link of MTDC transmission system. 51

Figure 3.3: Flowchart of the proposed TW based primary protection and DC fault location algorithm compliant to IEC 61869-9 measurement protocol. 52

Figure 3.4: Test MTDC transmission system. 53

Figure 3.5: Measurement of EPTs at DC terminal 3 (a) Mode-1 DC voltage (V_{m134} waveform with different fault resistance), (b) AT detection of 10 Ω fault resistance induced TW, (c) AT detection of 100 Ω resistance fault induced TW, (d) AT detection of 200 Ω resistance fault induced TW. 56

Figure 3.6: Measurement of EPTs at DC terminal 4 (a) Mode-1 DC voltage (V_{m143} waveform with different fault resistance), (b) AT detection of 10 Ω fault resistance induced TW, (c) AT detection of 100 Ω resistance fault induced TW, (d) AT detection of 200 Ω resistance fault induced TW. 57

Figure 3.7: (a) Mode-1 DC voltage of cable L_{34} at DC terminal 3 with 10 Ω , 100 Ω and 200 Ω fault resistance, (b) Current in HDCCB of DC link L_{34} for 10 Ω , 100 Ω and 200 Ω fault resistances. 58

Figure 3.8: At DC terminal 3 (a) Mode-1 DC voltage with 55 dB SNR noise, (b) Mode-1 DC voltage with 45 dB SNR noise, (c) Mode-1 DC voltage with 35 dB SNR noise, (d) TWAT detection for 55 dB SNR contaminated DC voltage signal, (e) TWAT detection for 45 dB SNR contaminated DC voltage signal, (f) TWAT detection for 35 dB SNR contaminated DC voltage signal. 60

Figure 3.9: $|AT_{34} - AT_{43}|$ estimation by the proposed protection scheme for 150 Ω DC fault in cable link L_{34} with varying fault location (a) for 500 kHz sampling frequency, (b) for 96 kHz sampling frequency, (c) for 50 kHz sampling frequency. 64

Figure 3.10: $|AT_{34} - AT_{43}|$ estimation by the proposed protection scheme for 150 Ω DC fault in cable link L_{42} with varying fault location (a) for 500 kHz sampling frequency, (b) for 96 kHz sampling frequency, (c) for 50 kHz sampling frequency. 64

Figure 3.11: Impact of sampling frequency and fault location on proposed fault localization performance for fault on DC cable L_{34} 65

Figure 3.12: (a) Time stamps in transients of DC voltage waveform at DC terminal 3, (b) TWAT estimation by the proposed TWAT extraction technique, (c) HDCCB clearing DC fault and recovering DC pole voltage. 68

Figure 3.13: At DC terminal 3 (a) Mode-1 DC voltage with PPG fault, (b) Mode-1 DC voltage with PPG fault, (c) Mode-1 DC voltage with NPG fault, (d) TWAT detection for PP fault condition shown in (a), (e) TWAT detection for PPG fault condition shown in (b), (f) TWAT detection for NPG fault condition shown in (c). 70

Figure 3.14: External fault at DC cable L_{24} (a) Mode-1 DC voltage at DC terminal 3, (b) TWAT estimation by the proposed scheme at DC terminal 3, (c) Mode-1 DC voltage at DC terminal 4, (d) TWAT estimation by the proposed scheme at DC terminal 4. 72

Figure 3.15: Impact of grid parameter changes (a) Abrupt change in active reference setting of MMC converter 4, (b) DC voltage waveform at DC terminal 4, (c) RS output at DC terminal 4 (no fault induced TW detection). 74

Figure 3.16: Comparison of proposed method with MMG and s-transform based protection and fault localization scheme (a) Mode-1 DC voltage at DC terminal 3 and 4 and mode-0 DC voltage at DC terminal 3, (b) TWAT estimation by MMG tool for modal signal in (a), (c) TWAT detection by MMG tool for mode-1 signal in (a), (d) No TW detection by S-transform output for modal signal in (a) under 35 dB noise, (e) TWAT estimation by S-transform output for modal signal in (a) under 50 dB noise, (f) TWAT estimation by S-transform output for modal signal in (a) under 50 dB noise, (h) Mode-1 DC voltage at DC terminal 3 and 4, (i) TWAT estimation for modal signal in (h) by proposed technique, (j) TWAT estimated for modal signal in (h) by proposed technique. 75

Figure 3.17: Four terminal symmetric monopole MTDC transmission system. 78

Figure 3.18: (a) Schematic outline of CHIL test setup, (b) CHIL setup of RTDS and TI TMS320f28379D (IED) protection unit. 79

Figure 3.19: (a) Mode-1 DC voltage and RS signal at DC terminal 8, (b) Mode-1 DC voltage and RS signal at DC terminal 9. 80

Figure 3.20: (a) AT of the first TW at DC terminal 8, (b) AT of the first TW at DC terminal 9, (C) CB trip signal sent to HDCCB located at DC cable between DC bus 8 and 9. 80

Figure 4.1: Simple two terminal HVDC transmission system. 86

Figure 4.2: (a) Pulse signal. (b)Reconstructed signal by SMPM and STDFT, (c) Complex frequency extracted by SMPM for the pulse signal, (d) Fault-induced TW, (e) Time index damping factor diagram with linear regression to detect zero crossing point 89

Figure 4.3: Test MTDC transmission system. 92

Figure 4.4: (a) Mode-1 DC voltage at DC terminal 3 with 500 kHz sampling frequency, (b) AT of the fault induced TW at DC terminal 3 for 500 kHz sampling frequency, (c) Mode-1 DC voltage at DC terminal 3 with 50 kHz downsampled frequency, (d) AT of the fault induced TW at DC terminal 3 for 50 kHz sampling frequency. 94

Figure 4.5: Impact of fault resistance on proposed TWAT estimation performance (a) Mode-1 DC voltage signal with 10 Ω , 50 Ω and 100 Ω PTG fault resistance at a distance of 120 km from DC substation 3, (b) AT estimation using proposed TWAT estimation technique for 10 Ω fault resistance, (c) AT estimation using proposed TWAT estimation technique for 50 Ω fault resistance, (d) AT estimation using proposed TWAT estimation technique for 100 Ω fault resistance. 97

Figure 4.6: Impact of noise interference on proposed TWAT estimation performance (a) Mode-1 DC voltage without noise interference, (b) Mode-1 DC voltage voltage with 40 dB noise interference, (c) TWAT estimation for v_{m134} without noise interference, (d) TWAT estimation for v_{m134} with 40 dB noise interference. 98

Figure 4.7:	Comparative analysis (a) Mode-1 DC voltage at DC terminal 3 for fault at 70 km from DC substation 3, (b) IMF (4 th level) for mode-1 signal in (a), (c) TWAT for 1 st arrival TW for 500 kHz sampling frequency measured mode-1 DC voltage signal in (a), (d) TWAT for 1 st arrival TW for 50 kHz sampling frequency derived mode-1 DC voltage signal in (a), (e) Mode-1 DC voltage at DC terminal 3 for fault at 2 km distance from DC substation 3, (f) IMF (4 th level) for mode-1 signal in (e), (g) TWAT for 1 st arrival TW for 500 kHz sampling frequency measured mode-1 DC voltage signal in (e), (h) TWAT for 1 st arrival TW for 50 kHz sampling frequency derived mode-1 DC voltage signal in (e).	100
Figure 5.1:	(a) Reconstructed pulse signal (TW) by SMPA and STDFT with the same number of terms of sinusoids. (b) Pulse-shape signal and sliding window. (c) Complex frequencies extracted by applying SMPA to the pulse shown in (b).	107
Figure 5.2:	(a) Aerial mode voltage signal (u_α). (b) Damping factor-time diagram obtained by applying fast improved SMPA algorithm. (c) The fitted line to the dispersed damping factors (using linear regression), and its ZCP (TWAT) estimation.	109
Figure 5.3:	Locus of symmetric point S_z in graph G.	112
Figure 5.4:	(a) Schematics of proposed WABPS for test hybrid AC/DC grid interfacing offshore wind farm. (b) Associated sectionalized graph representation.	117
Figure 5.5:	SMPA performance (a) u_α at DFR "A", (b) TWAT at DFR "A", (c) u_α at DFR "B", (d) TWAT at DFR "B", (e) u_α at DFR "C", (f) TWAT at DFR "C", (g) u_α at DFR "D", (h) TWAT at DFR "D", (i) u_α at DFR "E", (j) TWAT at DFR "E", (k) u_α at DFR "F", (l) TWAT at DFR "F", (m) u_α at DFR "G", (n) TWAT at DFR "G", (o) u_α at DFR "H", (p) TWAT at DFR "H", (q) u_α at DFR "I", (r) TWAT at DFR "I".	120

Figure 5.6: Impact of fault impedance on the proposed fast SMPA based TWAT estimation (a) TWAT at DFR "B" for 20 Ω fault resistance, (b) TWAT at DFR "B" for 60 Ω fault resistance, (c) TWAT at DFR "B" for 100 Ω fault resistance. 122

Figure 5.7: Impact of fault type on the proposed fast SMPA based TWAT estimation (a) TWAT at DFR "D" for LG fault type, (b) TWAT at DFR "D" for LL fault type, (c) TWAT at DFR "D" for LLL fault type. 123

Figure 5.8: LVRT control characteristics of MMC controller 126

Figure 5.9: Impact of LVRT control on conventional distance protection scheme (a) Reactive power flow from MMC 2 & L_{23} from bus 3, (b) Active power flow from MMC 2 & L_{23} at bus 3, (c) Current contribution from MMC 2, (d) Current contribution from L_{23} at bus 3, (e) AC voltage at MMC 2, (f) AC voltage at bus 3, (g) DC current in HVDC link, (h) DC pole voltage at MMC 1 and MMC 2 terminal, (i) Z_{app} seen by Relay R_1 with and without HVDC LVRT controller 127

Figure B.1: Graph diagram representation for *Lemma II* 136

Nomenclature

Abbreviations

ACCB	AC circuit breaker
ADC	Analog to digital
AFL	Actual fault location
AT	Arrival time
CHIL	Control hardware in loop
CFL	Calculated fault location
CTD	Coordinated time delay
CWT	Continuous wavelet transform
DFR	Digital fault recorder
DPU	Data processing unit
EPT	Electric potential transducer
FCL	Fault current limiter
FLE	Fault location error
GTDI	Giga-transceiver digital input
GPIO	General purpose input/output
GTAI	Giga-transceiver analog input
GTAO	Giga-transceiver analog output
GOOSE	Generic object oriented substation event
HDCCB	Hybrid DC circuit breaker
HVDC	High voltage direct current
HVAC	High voltage AC
IGBT	Insulated gate bipolar transistor
IMF	Intrinsic mode function

LCC	Line commutated converter
LG	Line-to-ground fault
LL	Line-to-line fault
LLL	line-to-line-to-line (three phase fault)
LVRT	Low voltage ride through
MTDC	Multi terminal high voltage direct current
MMC	Modular multilevel converter
MUDW	Morphological un-decimated wavelet
MMG	Mathematical morphological gradient
NPG	Negative pole-to-ground
OCT	Optical current transducer
OHTL	Overhead transmission line
OCCO	Opening-closing-closing-opening filter
PTP	Precision time protocol
PCA	Principal component analysis
PP	Pole-to-pole fault
PPG	Positive pole-to-ground fault
PMU	Phasor measurement unit
PCC	Point of common coupling
ROCOV	Rate of change of voltage
RTDS	Real time digital simulator
SE	Structure element
STDFT	Short time discrete Fourier transform
SVD	Singular value decomposition
SNR	Signal-to-noise-ratio
SATD	Surge arrival time difference
SMPM	Sliding matrix pencil method
TW	Traveling wave
TWAT	Traveling wave arrival time
VSC	Voltage source converter
VMD	Variational mode decomposition
VF	Velocity factor

WABPS	Wide area backup protection scheme
ZCP	Zero crossing point

Symbols and variables

ψ_i^\uparrow	Signal analysis operator
ψ_i^\downarrow	Signal synthesis operator
ω_i^\uparrow	Detail analysis operators
δ	Dilation operator
ε	Erosion operator
γ	Opening operator
i_d	Identity operator
ϕ	Closing operator
\oplus	Dilation operation
\ominus	Erosion operation
\circ	Opening operation
\bullet	Closing operation
Z_{in}	Internal zone
Z_{fe}	Forward external zone
Z_{be}	Backward external zone
x	per unit length of transmission line
ζ	Threshold value
Δt	Sampling time period
M	length of SE
α	Damping factor
β	Phase constant
α_S	Skin-effect loss in TW
α_D	Dielectric loss in TW
α_G	Conductivity of dielectric loss in TW
α_R	Radiation loss in TW
Σ	Diagonal matrix containing the singular or eigenvalues of Matrix in SVD
p	Filtering parameter
L	Pencil parameter

σ	Singular value
R	Left side unitary matrix of SVD
S	Right side unitary matrix of SVD
b	Regression coefficient
n	Nodes of graph theory
b	Branches of graph theory
w	Weight of branches in graph theory
P_{n_1, n_2}^{min}	Shortest path between two nodes n_1 and n_2
g	Graph network
D_{n_1, n_2}	Distance between nodes n_1 and n_2
l_x	length of x transmission line
t_x	TWAT at bus x
v_{TW}	velocity of traveling wave
v_{m0}	mode-0 DC voltage
v_{m1}	mode-1 DC voltage
i_{m0}	mode-0 DC current
i_{m1}	mode-1 DC current
v_p	Positive pole DC voltage
v_n	Negative pole DC voltage
i_p	Positive pole DC current
i_n	Negative pole DC current
P_x	Polarity of traveling wave at x
f_1	Sampling frequency is 500 kHz (High)
f_2	Sampling frequency is 50 kHz (Low)
u_α	Aerial mode signal of Karenbauer transformation
u_β	Aerial mode signal of Karenbauer transformation
u_0	Ground mode signal of Karenbauer transformation